NEW ACOUSTIC WAVE PIPE INSPECTION SYSTEM

Venugopal K. Varma, Raymond Tucker, Steve Kercel,
Thomas Thundat, and Ali Passian
Oak Ridge National Laboratory

Joseph Rose and Xiaoliang Zhao
Pennsylvania State University

INTRODUCTION

The safety of the Unites States' natural gas supply is of prime importance since 30% of the energy produced in the country is derived from it. Natural gas is supplied through a million miles of vast pipeline network. Pipeline companies have an impressive safety record due to the proactive role of standards and inspection of pipelines. Since the pipelines are getting old, there is a great need to identify corrosion, cracks, and other defects that can cause potential problems.

Stress corrosion cracking (SCC) can occur under a range of pipeline field conditions including soil type, stress, cathode potential, coating conditions and temperature. This type of defect is usually oriented along the lengthwise direction of the pipe. If not found and conditions persist, the cracks may grow and/or coalesce and eventually result in a leak or pipe rupture. There are also other types of defects that can occur in pipe structures. They are either critical to the safety of the pipeline like corrosion, welding cracks, pits etc or benign stringer-like internal inclusions. Non-destructive Inspection (NDI) systems are strongly needed to be able to locate the defects early without false alarms from benign inclusions, and to characterize and size the defects for repair or replacement management.

Many technologies have been developed for pipe inspections, but they are limited to detecting certain types of defects. For example, Axial-field Magnetic Flux leakage (MFL) in-line inspection smart pipe-inspection-gears (PIGs), extensively used for pipeline inspection, are good for detecting corrosion damage or circumferentially oriented defects inside a pipe. It is not suitable for detecting flaws or cracks in the axial direction.

In this project, ultrasonic guided waves are being studied for the feasibility of detecting many kinds of defects that occur in pipes. One major benefit of guided waves is their rapid global inspection capabilities which enables them to inspect a structure line-by-line instead of point-by-point. However, defect classification and sizing by guided waves are still a major problem under investigation due to the complexity of the wave propagation characteristics.

MODELING

2D MODELING

BEM (Boundary Element Method) analysis is used to model the flaws and study the effect of guided shear waves impinging on the flaw. The dispersion curves of the circumferential guided.

Shear (SH) waves were calculated to arrive at the EMAT settings for generating n1 mode. Comparison of the dispersion curves with those of a flat plate shows that a large diameter thin walled pipe can be approximated as a plate locally (see Fig. 1). The transmission and reflection coefficient for the shear wave incident on a crack 1/8 in. wide are as shown in Fig. 2. These were calculated using 2-D BEM analysis.

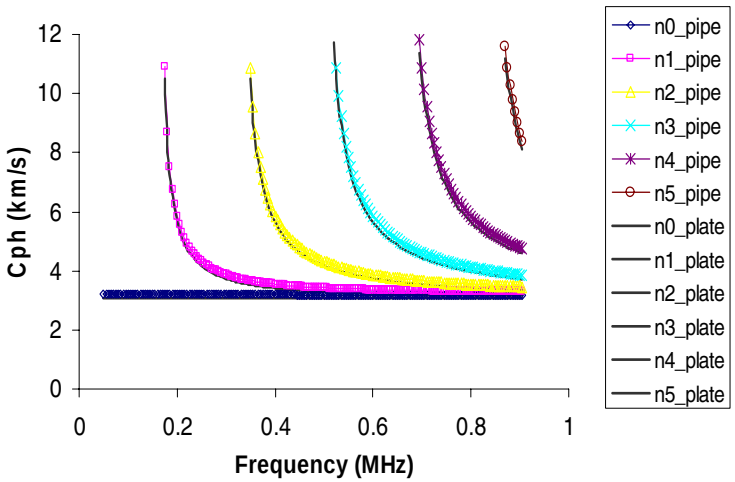

Fig. 1. Phase velocity dispersion curves for SH wave in the circumferential direction of a 10 in. schedule 40 steel pipe and plate of same thickness (9.271 mm).

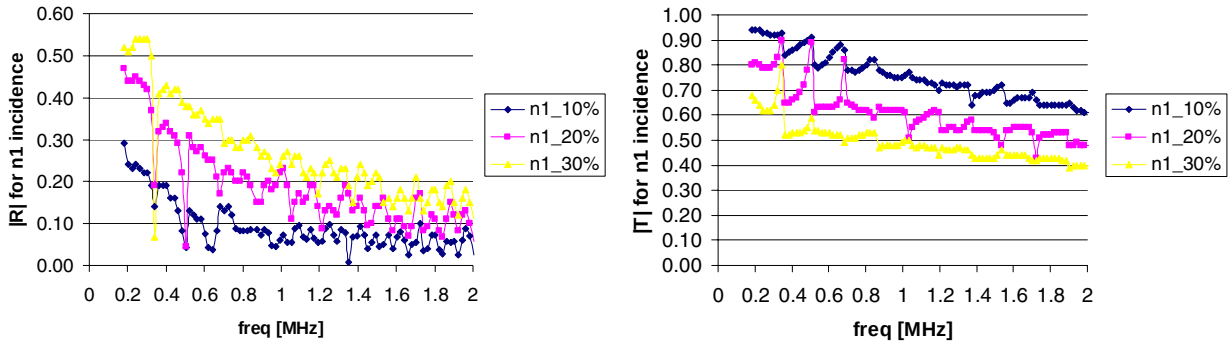

(a) **(b)**

Fig. 2. (a) The reflection coefficient and (b) transmission coefficient of n1mode for n1mode SH wave incident into 1/8 in. wide cracks with 10%, 20%, and 30% through wall depth. The pipe wall is 9.272 mm thick.

3D MODELING OF FLAWS

The geometry for the 3-D problem can be shown in Fig. 3. A cylindrical coordinate system is attached to the center of the meshed disc region, with the z = 0 plane being the mid-plane of the plate. A commercial Finite Element Analysis package called IDEAS was used to mesh the surface of the disc with defects. Quadrilateral 2-D elements were used. The software package can output the coordinates of each corner points and the connectivity relation between elements and corner points were also given. This information can be input to the 3-D BEM code as geometry mesh. Consider a time-harmonic SH plane wave incident from the left, the scattered wave field may consists Lamb waves and SH waves.

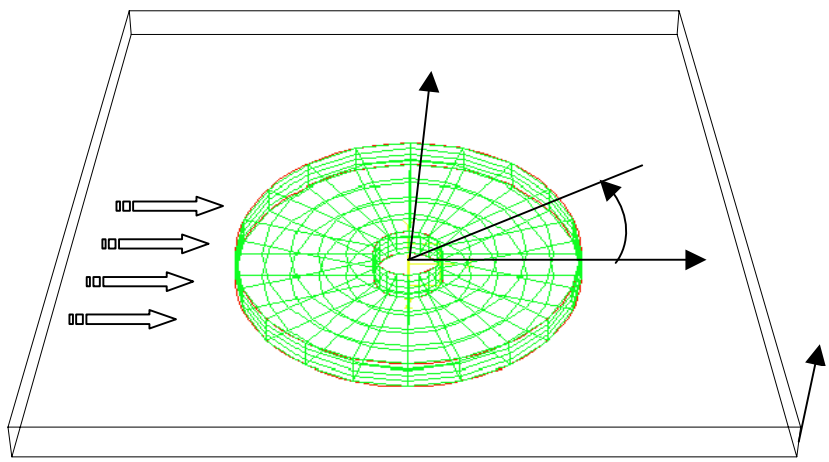

Fig. 3. An example mesh for three-dimensional defects in an infinite plate and the coordinate system set-up. A plane SH wave is incident onto the defect region.

BEM CALCULATION OF SCATTERED GUIDED WAVE FIELD FROM A THROUGH-PLATE HOLE

The hybrid boundary element normal mode expansion technique was applied to the calculation of the scattered wave field from a circular through-plate hole in a plate (see Fig. 3). Note that this defect can be substituted by any arbitrary shaped 3-D defect without jeopardizing the validity of the code. The geometry mesh used here is just for testing the concept with an easy mesh. Considering a plane shear horizontal wave propagating in the positive x direction, it impinges onto the defect and will be scattered back. The scattered wave consists of all propagating as well as non-propagating modes of both the Shear Horizontal wave and the mode converted Lamb wave. The non-propagating waves do not carry away any energy flux and die out within several wavelengths. Thus only propagating modes exist beyond the virtual boundary, which was chosen to be far enough (usually much larger than a wavelength) from the defect. Figure 4 (a), (b), and (c) show the x, y, and z component of the scattered wave particle displacement amplitude on the outer cylindrical surface, respectively. In each figure, the amplitude curves of three frequency points were displayed. The red dot-dash line with an arrow still shows the positive x direction.

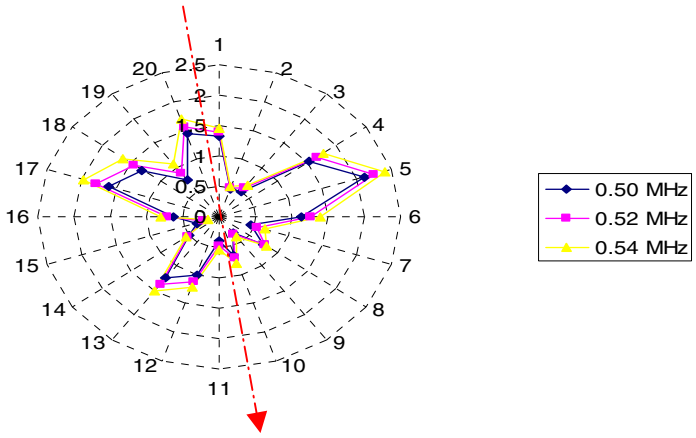

(a)

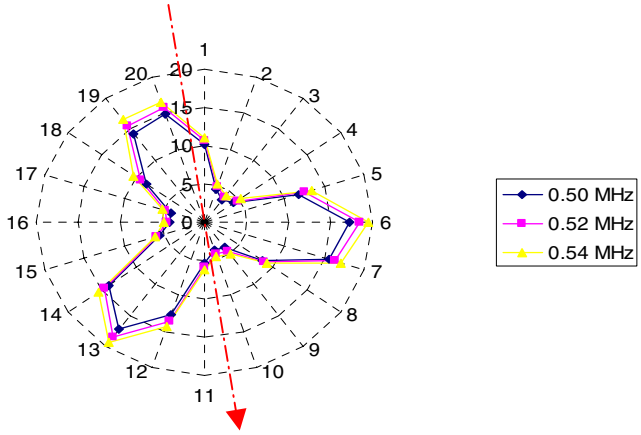

(b)

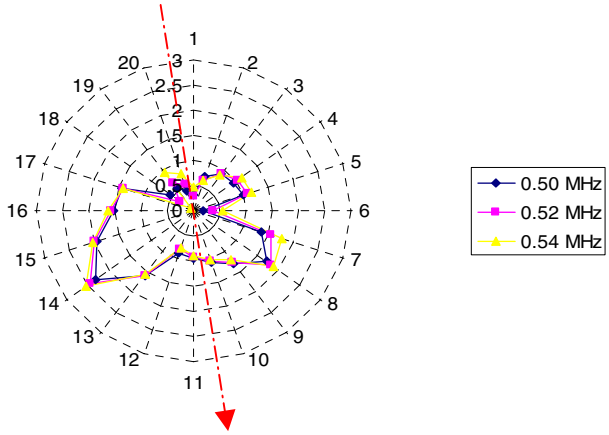

(c)

Fig. 4. (a) x component of the scattered wave particle displacement amplitude on the outer cylindrical surface. The red dot-dash line with an arrow shows x direction. (b) y component of the scattered wave particle displacement amplitude on the outer cylindrical surface. The red dot-dash line with an arrow shows x direction. (c) z component of the scattered wave particle displacement amplitude on the outer cylindrical surface. The red dot-dash line with an arrow shows x direction.

It is seen the displacement components are not strictly symmetric with respective to the x axis anymore. This might due to the asymmetric boundary conditions. Further studies will be conducted on this. The three curves of different but close frequency show similar scatter patterns, which may indicate good stability of the code developed. Further study will be carried out to decompose the scattered field into normal modes and to give the scattering or mode conversion coefficients.

EMAT EXPERIMENTAL SET-UP

EMAT sensors were designed for 10 in. and 12 in. pipe geometry with hardware fabricated for attaching them on to the inside walls of the pipe. The anchoring mechanism had provisions to vary the gap between the pipe wall and the EMAT. With wheels/ball rollers, the EMATS could be positioned anywhere inside the pipe. Figure 5 shows the circumferential and axial EMATS developed for pipeline inspection.

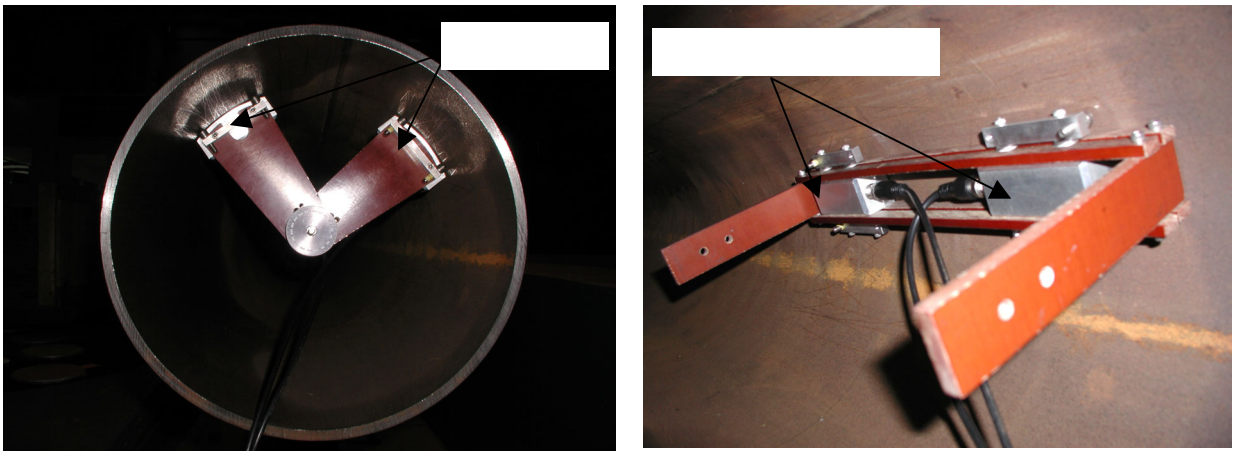

Fig. 5. Axial and Circumferential EMATs.

1/8 in., 1/4 in., and 0.006 in. wide cuts with varying depths were fabricated on the pipe walls to determine whether the EMATS are able to detect these flaws. Most tests were performed using horizontal n1 mode shear wave. By utilizing the through transmission mode whereby the distance between the EMATs is fixed, better correlation was obtained for the effect of flaws. A sample of the windowed receiver pulse signal for the case of no-flaw and flaws on the pipe walls is given in Fig. 7. As can be seen from the figure, the signal is strongest when there is no flaw and reduces in amplitude when it encounters a flaw. The multiple pulses in Stress Corrosion Cracks (SCC) flaw data is due to the smaller section of the pipe (18 in. instead of 6 ft) used for this case. These pulses correspond to the reflections from the pipe ends and are separated by larger time intervals when the pipe section used is long. Number of EMATs required to characterize the entire diameter of the pipe was determined by assessing the propagation angle

that does not affect the quality of the signal for preset EMAT separation. Fixture in Fig. 6 was used to perform these experiments.

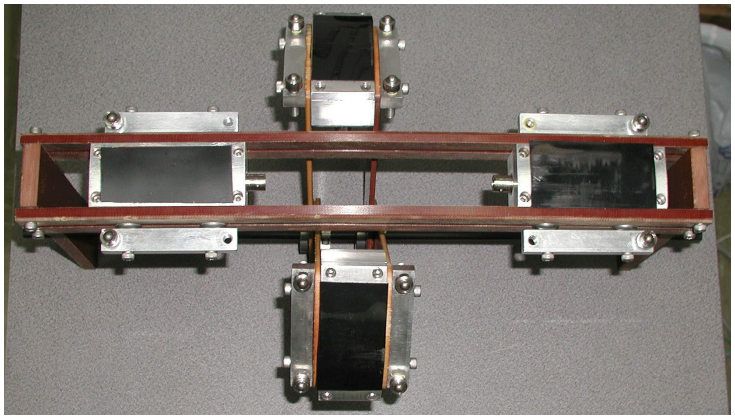

Fig. 6. Fixture for attaching both circumferential and Axial EMATs.

Attenuation or changes in amplitude in the time domain data (see Fig. 7) are not a useful feature for identifying flaws. Despite the fact that such changes are obvious in laboratory data collected under carefully controlled conditions, their reliability does not hold up for data collected in less controlled field conditions. Too many other mechanisms besides a flaw in the medium of propagation can lead to attenuation in field data. The only reliable features for flaw detection are those that depend on the change imposed by the flaw on the shape rather than the amplitude of the signature.

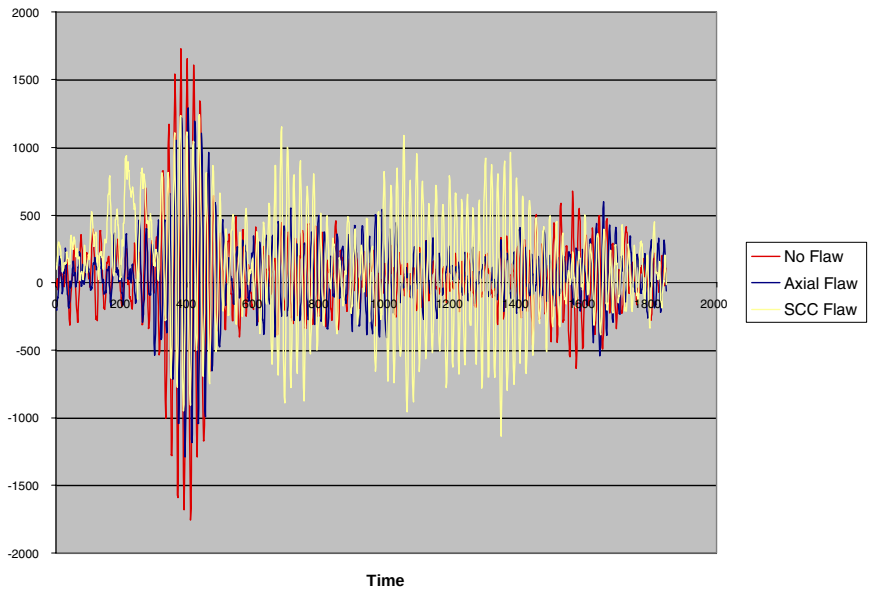

Fig. 7. Amplitude Versus Time for Flaw and No-flaw Receiver EMAT Signal.

SIGNAL ANALYSIS

To find features that distinguish the presence of a flaw, the signal must be analyzed, or literally broken apart. Since the EMAT-induced ultrasonic signature is an oscillating transient burst of energy, and the problem is to consider how a flaw in the propagation medium disrupts the pattern of the burst. A reasonable approach is to break up the signal into pieces that are themselves oscillating transient bursts. Discrete wavelet transform was used for this analysis.

The idea in pattern recognition is that the "no-flaw" signals will all be similar to each other. They will concentrate in a bounded region of feature space relatively close to a cluster center. In the case of an N-dimensional feature space, if the feature dimensions were on the same scale, the feature vectors for the "no-flaw" signals would form a cluster inside some N-dimensional hypersphere whose center is the "cluster center," and is located at the mean of the feature vector values of all the no-flaw samples. "Flaw" signals will have feature vectors that are scattered all over the feature space and at some distance from the "no-flaw" cluster center, outside the hyperspherical "decision surface."

The feature space can be transformed by rotating its coordinate axes to align with the eigenvectors of the covariance matrix of the "no-flaw" features and rescaling all axes to the same scale. As a result, the distance of any feature vector from the cluster center can then be represented as a single number, conventionally known as the Mahalanobis distance (Fig. 8).

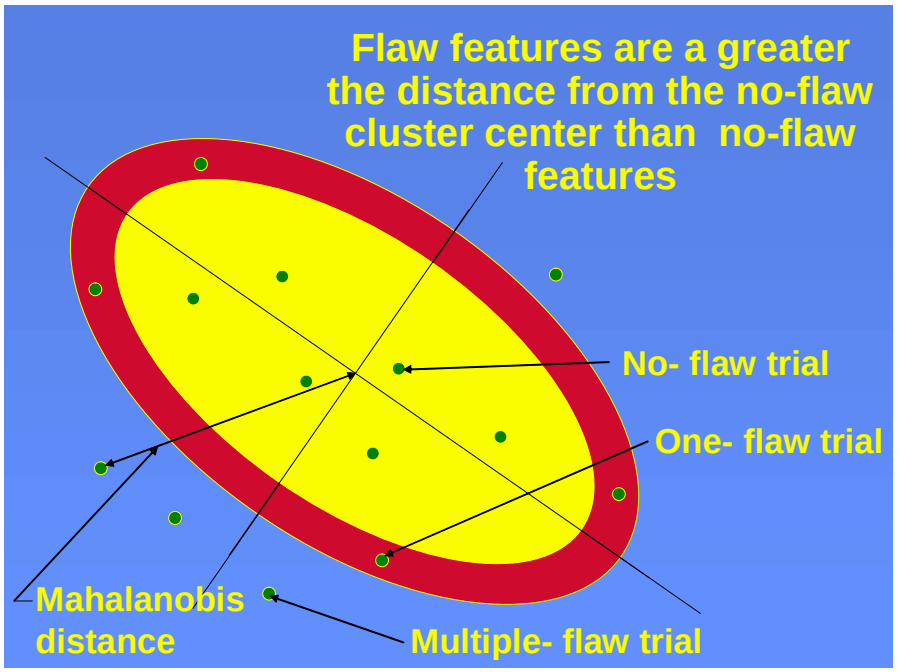

Fig. 8. Clustering of Features.

The above wavelet analysis was performed on the data obtained using shear EMATs on 10 in. and 12 in. diameter pipes with fabricated flaws. Figure 9 shows the classification SCC flaws. The horizontal axis is the fraction of signal energy retained in wavelet-packet space for the analysis. The vertical axis is the squared Mahalanobis distance of the feature vector from the cluster center of the “No Flaw” samples. There is one line on the graph for each trial. The line represents the Mahalanobis distance of the feature vector from the “no flaw” cluster center, as a function of retained energy.

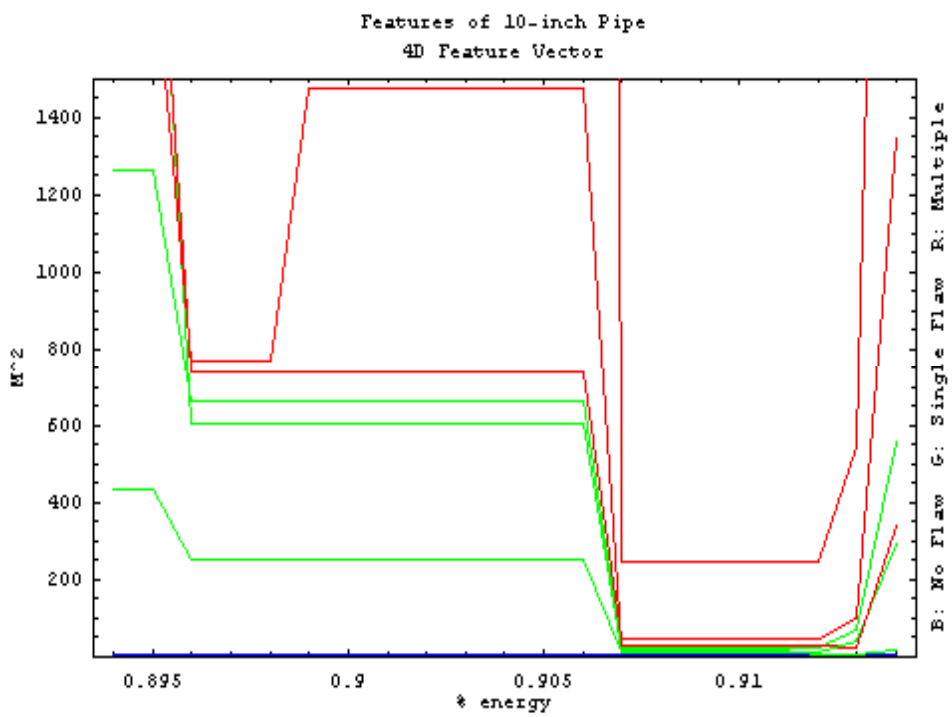

Fig. 9. Mahalanobis distance for SCC Flaws.

Signatures for the 10-in. pipe were fully distinguished into three classes (no flaw, single flaw, and multiple flaws) by an analysis similar to that described above. The wavelet filter used for processing is an 8-coefficient Least Asymmetric Wavelet.

MICROCANTILEVER LEAK DETECTION

A novel MEMS-based acoustic sensor that uses an array of high Q microcantilevers, such as those used in atomic force microscopy is being developed for internal and external acoustic detection of ultrasound emitted from defects (holes and cracks) in pressurized gas systems such as gas pipelines. It is essential to monitor the integrity of commercial pipelines for defects that can cause potential problems in the future, as well as to identify existing defects that are currently causing problems. It is conceivable that detecting and characterizing the flaws will help determine potential leakage in a pipe, but a sensor tuned

to the sound frequency generated by the gases escaping from the pipe gives a positive identification of the leak. Modern leak-detection systems for pipelines are usually bulky, expensive and rely upon often inaccurate or time consuming detection methods such as flow rate analysis, mass difference calculations or trace gases. In comparison, a system utilizing microcantilevers would occupy a smaller footprint either within the pipeline, or outside it and will enable the integrity of the pipe to be assessed without evacuation.

Acoustic detection using microcantilevers can be accomplished using a micromachined silicon cantilever with typical dimensions of 100 μm length, 20 μm width, 0.3–1 μm thickness, with a Q-factor of 100. The fundamental resonance frequency, **f**, of an oscillating cantilever can be easily shown to be expressed by $\omega = (k/m_e)^{1/2}$, where **k** is the equivalent spring constant and m_e is the effective mass of the cantilever beam. The spring constant is determined by the geometrical and material properties of the beam. For a rectangular cantilever, response to acoustic energy occurs primarily along the axis parallel to a normal to the cantilever. This translates into directionality capabilities as shown in the results presented below.

In order to determine the resonance frequency of the cantilever, we monitor the cantilever response, and the driving signal to the acoustic transducer simultaneously on a spectrum analyzer. By frequency sweeping the driving voltage (<1 volt peak-to-peak) of the transducer from the signal generator in the initial interval 15–100 kHz at a rate of 2 KHz per second, and an iterative reduction of this interval centered at the observed frequency response of the cantilever, the fundamental resonance frequency was determined at the maximum of the Q factor. With a bias voltage of V = 5 volts, a nominal cantilever resistance of $R_c = 2.2$ kΩ, and with the transducer plane parallel to the cantilever plane and positioned 20 cm away, the fundamental resonance frequency in air at room temperature was measured. This is summarized in Fig. 10. As the width of the sweeping in Fig. 10a is reduced, the resonance peak of the cantilever is measured from the sharp peak in Fig. 10b. As can be seen, for this cantilever, the peak is at f = 22.50 kHz, and therefore the quality factor $Q = f/(\Delta f)|_{FWHM}$ can be determined at FWHM of ≈128 Hz to be Q = 176. We note here that the FWHM of the driving voltage to the transducer was less than 40 Hz. The peaks for most examined cantilevers appear to be in the range $22 < f < 50$ kHz, i.e., in the ultrasound region.

The maximum amplitude of each frequency peak of the cantilever in Fig. 10 is directly proportional to the amplitude of the effective driving force F exerted by the pressure fluctuations in the driving acoustic field.

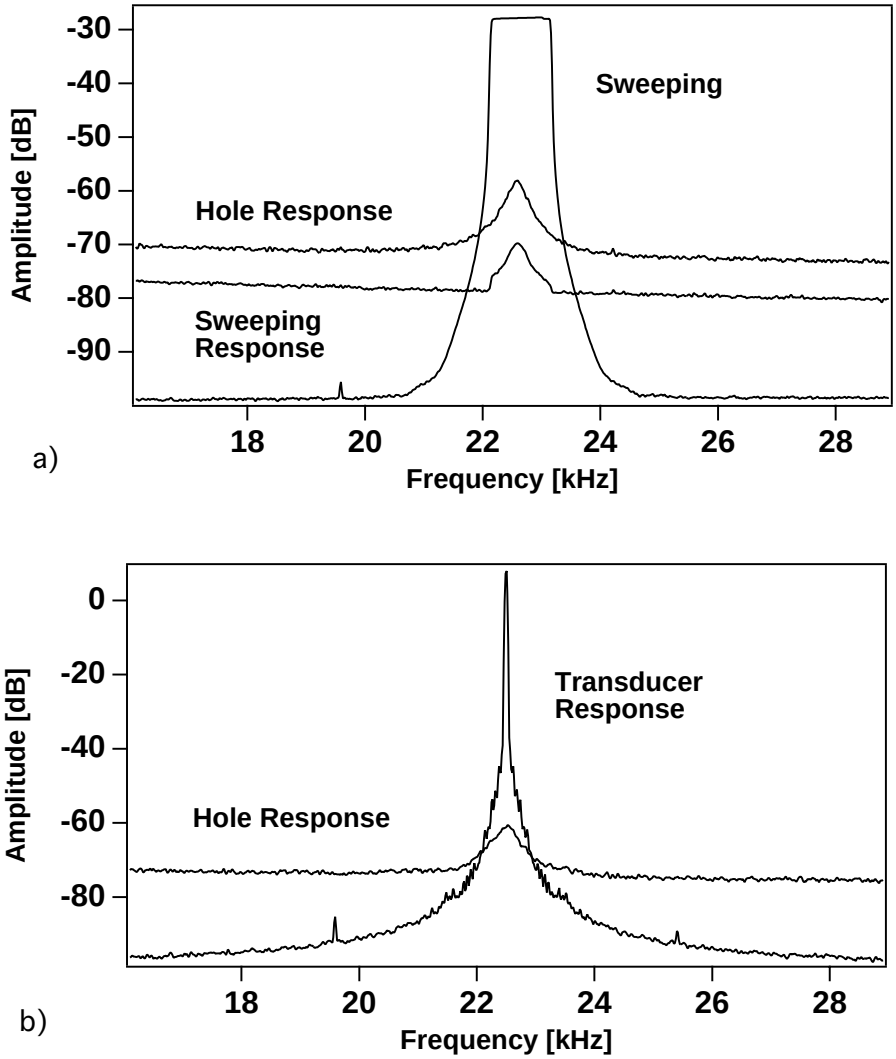

Fig. 10. Frequency response of the cantilever.

REFERENCES

Passian, A., Evans, P. G., Varma, V. K., Ferrell, T. L., and Thundat, T., "Piezoelectric detection of acoustic waves," Review of Scientific Instruments, Vol.74, No.2, February, 2003.

Tucker, R. W., Kercel, S. W., and Varma, V. K., "Characterization of gas pipeline flaws using wavelet analysis," QCAV (Quality Control Using Artificial Intelligence), Gatlinburg, TN, May 2003.

Kercel, S. W, Tucker, R. W., and Varma, V. K, "Pipeline flaw detection with wavelet packets and Gas," SPIE 2003.